INFLUENCE OF PLASTIC STRAINS ON THE MECHANICAL PROPERTIES OF STAINLESS STEEL SHEETS

A. Gehring, H. Saal, J. Schmied

Universität Karlsruhe (TH), Germany

Abstract

Recently the computational power is rising rapidly. This allows even in complex engineering problems to predict a more accurate response of a system due to loading by using numerical simulations with sophisticated material models. For instance the spring back behaviour of complex auto body parts in sheet metal forming predicted by using combined isotropic/kinematic hardening models as well as strain dependent Young's modulus agrees with experimental results. Also the ultimate limit state of thin-walled cold-formed sections with variable loading conditions is predicted more precisely. However, the problem in practical application is, that the characteristic material parameters required for the sophisticated material models implemented in commercial finite element codes are difficult to determine. This is due to the missing experimental procedures and the complexity of the problem.

In this paper, the mechanical material properties of austenitic stainless steel 1.4301 sheets in annealed condition are investigated. The focus is on the kinematic hardening behaviour and the dependence of Young's modulus on plastic strain. The experimental methods are those used in investigations into the behaviour of carbon steels and aluminium alloys. The dependence of Young's modulus on plastic strain is determined by a procedure proposed by Busche [2]. The kinematic hardening behaviour is investigated with an experimental procedure proposed by Gehring and Saal [4]. A nonlinear combined isotropic/kinematic hardening proposed by Chaboche [1] is used for the evaluation of the results. The results of the investigation are discussed with respect to existing results for carbon steel grades. Also the material model proposed for finite element application in EN 1993-1-4, Annex C [7] is discussed with regard to the results of the experimental results.

Introduction

The application of cold-formed stainless steel sections in buildings is rising continuously due to the good corrosion resistance and the low maintenance costs over the full life cycle of a component. The resistance of thin gauged cold-formed cross-sections can be determined with calculations based on the effective width approach according to international design codes, e.g. EN 1993-1-4 [7]. The application of the design codes leads to conservative resistance values. The full benefit of the cross-sectional resistance can be achieved only by cost intensive experimental investigations, e.g. according to the guidelines given in EN 1993-1-3 [8]. This procedure takes a lot of time and is very cost intensive, especially if it includes modifications for optimising the component. Therefore finite-element analyses are performed to investigate the structural behaviour of a component in advance to production to reduce both costs and time. Within these virtual tests, the material properties are assumed to be distributed uniformly following the guidelines given in EN 1993-1-4 [7], which leads to a safe estimation of the failure loads. An enhanced yield strength due to cold-working is introduced into the analysis by

partitioning a cross-section [9]. However, the real distribution of the material properties is not covered by this approach. A new analysis strategy overcomes this problem by combining both the analysis of the manufacturing process and the analysis of the ultimate limit state of the component [10]. This accounts realistically for geometric imperfections, residual stresses and cold-working effects in the ultimate limit state analysis. However, this analysis strategy demands more accurate modelling of the mechanical material behaviour. In this paper, the mathematical formulation and the experimental identification of some properties are discussed and demonstrated with austenitic steel grade 1.4301 sheet.

Material model and parameter identificiation

Material model

Following the theory of plasticity, the total strain is decomposed into the elastic strain ε_e and the inelastic or plastic strain ε_p [1]. The constitutive relation for ε_e is Hook's law

$$\sigma_{ij} = C_{ijkl} \cdot \varepsilon_{kl} \tag{1}$$

where C_{ijkl} is the tensor of elasticity. Here, the elastic part is assumed to be isotropic and independent of the strain rate. From this follows, that C_{ijkl} is defined by Young's modulus E and Poisson's ratio ν. However, the value of Young's modulus E depends on plastic strain ε_p.
The plastic part is described with a material model including a kinematic and an isotropic hardening component proposed by Chaboche [1]. In this material model, the yield function is defined as

$$F = f(\sigma_{ij} - X_{ij}) - k_f = 0 \tag{2}$$

where σ_{ij} is the Cauchy-stress tensor, X_{ij} is the backstress tensor and k_f is the reference yield stress of the yield surface. A shift of the elastic domain in the stress space is described by the backstress tensor. A detailed description of the material model is given in [1].

Mathematical description of components

With carbon steels the dependence of Young's modulus on plastic strain ε_p can be described realistically with an exponential function [2], [3]. Here, the function

$$E(\varepsilon_p) = E_0 - A \cdot \left(1 - e^{-s \cdot \varepsilon_p}\right) \tag{3}$$

was chosen, where E_0 is the initial value of the Young's modulus, A and s are material constants. In case of an uniaxial loading, the backstress X depends on the accumulated plastic strain p in terms of

$$X(p) = \pm\frac{C}{\gamma} + \left(X_0 \mp \frac{C}{\gamma}\right) \cdot e^{\mp\gamma \cdot (p - p_0)} \tag{4}$$

where C and γ are material parameters [1]. The top sign corresponds to tensile and the bottom sign to compressive strains, X_0 and p_0 denote the initial values at the beginning of each plastic flow. The isotropic hardening can be expressed as a function of plastic strain p by

$$k_f(p) = k_{f0} + \sum_{i=1}^{k} Q_i \cdot \left(1 + e^{-C_i \cdot p}\right) \tag{5}$$

where Q_i and C_i are material parameters and k_{f0} is the initial yield stress. The necessary number k of the terms to be summed up depends on the shape of the flow curve to be fitted. Figure 1 shows schematically for the uniaxial case how the isotropic and the kinematic hardening component change with plastic strain p.

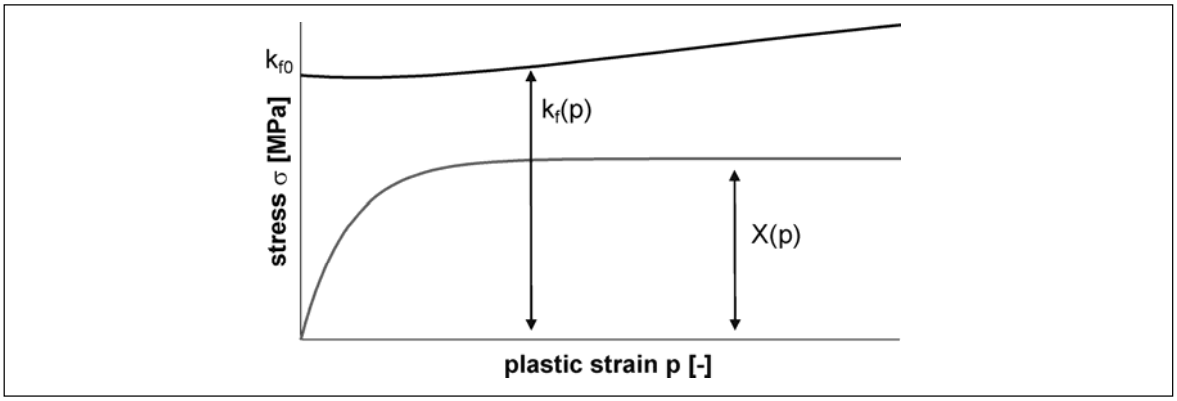

Figure 1. Schematic representation of the material model for uniaxial loading

Experimental parameter identification

The experimental methods are those used in investigations into the behaviour of carbon steels and aluminium alloys. A procedure proposed by Busche [2] is used to determine how Young's modulus depends on plastic strain. This is by a tensile test according to EN 10002-1 [5] using several pre-strained specimen taken from one batch. In addition Young's modulus at the initial state as well as that at uniform elongation is required. Here Young's modulus is determined according to EN 2002-001 [6], method 1.

Quasi-static reversed loading tests are performed to determine the parameters of the kinematic hardening component. For this it is recommended to perform tests with different strain amplitudes $\Delta\varepsilon_p/2$ on different levels of the mean strain ε_m [1]. The test procedure is shown in Figure 2 schematically. The jig used for testing is described in [4]. Here, all quasi-static reversed loading tests were performed under control of total strain.

In addition, the flow curve is determined in uniaxial tensile tests according to EN 10002-1 [5]. The parameters of the flow curve are determined by fitting Equation (4) to the experimental results using three terms of the sum in Equation (5). The evaluation of the results of the quasi-static reversed loading test is performed in three steps [1]:

- approximate determination of the yield stress k of a stress strain hysteresis, where k is not identical with the initial yield stress k_f from an uniaxial tensile test
- determination of C/γ as asymptotic value of $(\Delta\sigma/2) - k$ as a function of plastic strain p
- determination of C by fitting Equation (6) to the experimental results

$$\frac{\Delta\sigma}{2} - k = \frac{C}{\gamma} \cdot \tanh\left(\gamma \cdot \frac{\Delta\varepsilon_p}{2}\right) \tag{6}$$

A least-square algorithm is used for fitting Equation (3), (4), (5) and (6) to the experimental results.

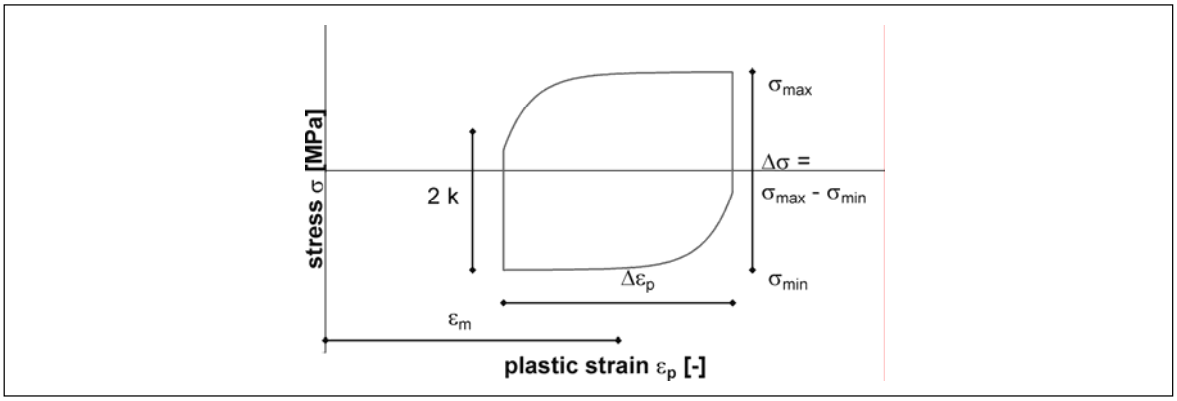

Figure 2. Testing procedure for quasi-static reversed load test

Extent of investigation and results

Steel grade

The change of Young's modulus and the kinematic hardening behaviour with plastic strain is investigated with specimen from cold rolled sheet in gauge 0,60 mm of austenitic stainless steel 1.4301 in annealed condition. All specimen are taken transverse to the direction of rolling. The tests were performed with specimen without pre-strain and with specimen which were pre-strained to 4 %, 8 %, 16 % and 32 % respectively. The characteristic material parameters of the batch are $R_{p0,2}$ = 200 MPa, R_m = 510 MPa and A_{80mm} = 71 %.

Results

Young's modulus

Figure 3 shows how Young's modulus depends on plastic strain. It decreases to approximately 75% of its initial value where this decrease is nearly complete with total strains less than 10%. It is obvious from Figure 3, that Equation (3) is well suited for a mathematical reproduction of the change of Young's modulus with the parameters E_0 = 228 GPa, A = 57 GPa and s = 22.

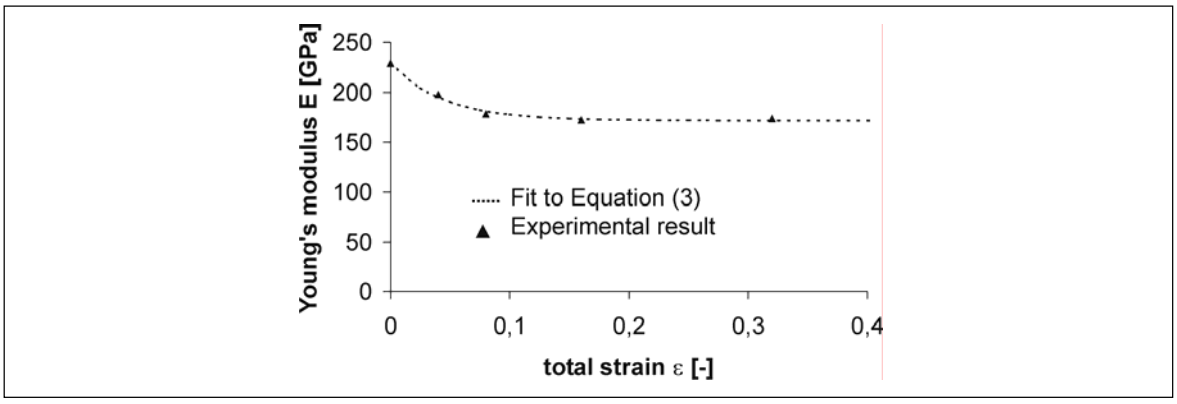

Figure 3. Change of Young's modulus of austenitic steel 1.4301 with total strain

Kinematic hardening behaviour

Figure 4 shows the isotropic and kinematic hardening behaviour in a range of small strains. It is obvious, that the evolution of the yield surface depends on the accumulated strain. Small strain amplitudes have no significant effect on the size of the yield surface. However, for large strain amplitudes the size of yield surface increases significantly from cycle to cycle.

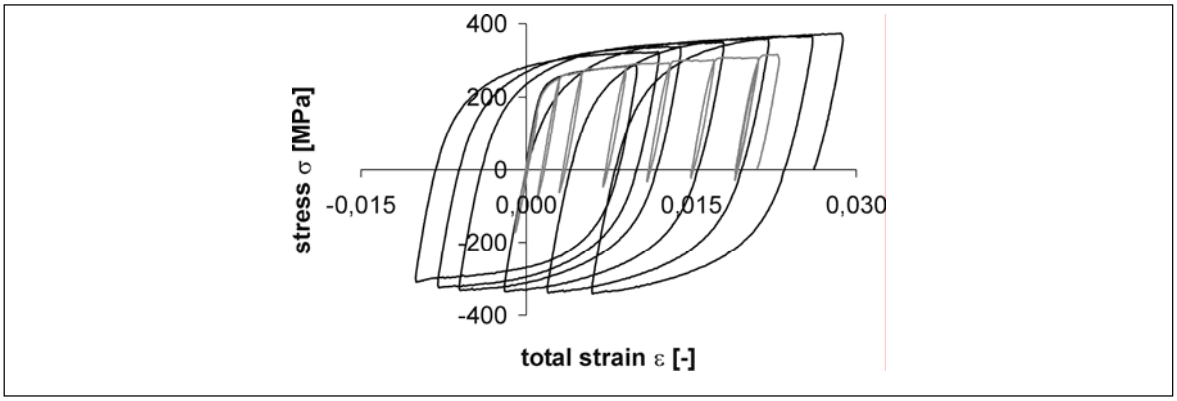

Figure 4. Stress-strain hystereses of austenic steel 1.4301 with different strain amplitude

Figure 5 shows how the backstress X varies with pre-strain. The ratio C/γ is increasing with increasing pre-strain. This is due to an increasing value of the kinematic hardening modulus C (from C = 234 GPa to C = 324 GPa). The exponent γ is decreasing from γ = 1882 to γ = 1127.

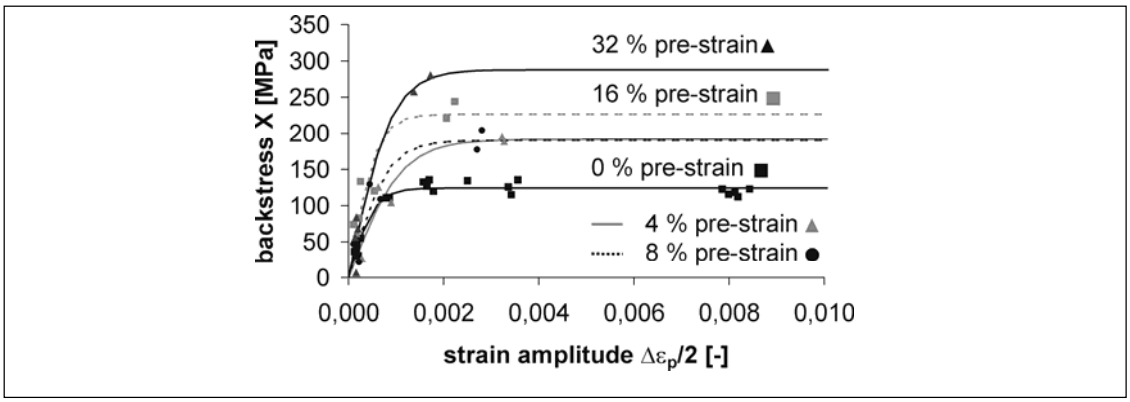

Figure 5. Backstress X for austenitic steel 1.4301 with different values of pre-strain

Discussion

The results show, that Young's modulus E and the parameters of the kinematic hardening compoment depend on plastic strain for austenitic stainless steel 1.4301. Young's modulus is decreasing with increasing plastic strain. The relation between Young's modulus and plastic strain agrees qualitativley with results obtained for different carbon steels and aluminium alloys [2]. For the parameters of the kinematic hardening component a comparison with other steels is difficult because only few results are published.

The approach in EN 1993-1-4, Annex C [7] for modelling the flow curve for finite element application does not account for these effects. The change of the material properties due to plastic strain has strong influence on the load bearing behaviour of cold formed products. This applies also for Young's modulus. That means, that the stiffness of a cold-formed component can be overestimated up to 25 % using the value of Young's modulus specified in EN 1993-1-4 [7].

This change also strongly influences the results of numerical analyses of the production process of cold-formed sections. The structural behaviour of cold formed sections will therefore only be reflected realistically if these effects of plastic strain on material properties are taken into account.

Summary

The mechanical properties of austenitic stainless steel 1.4301 were investigated. Especially properties, which are important for numerical analyses of cold-formed sections were analysed. The focus is on the change of Young's modulus and the parameters C and γ of the kinematic hardening behaviour with plastic strain. It is shown, that this change is significant. Young's modulus and the exponent γ is decreasing and the kinematic hardening modulus C is increasing with increasing plastic strain.

References

[1] J. Lemaitre, J.-L. Chaboche, Mechanics of solid materials, Cambridge University Press, Cambridge, 1994

[2] C. H. Busche, Bestimmung und Beschreibung des Elastizitätsmoduls von Blechwerkstoffen nach dem Umformen, Dr.-Ing. Dissertation, RWTH Aachen, 2006

[3] A. Krasovsky, W. Schmitt, H. Riedel, "Material characterization for reliable and efficient springback prediction in sheet metal forming", steel research international, 77, 2006,pp. 747 - 753

[4] A.Gehring, H. Saal, „Vorrichtung zur Prüfung von Feinblech unter Druckbeanspruchung", Materialwissenschaft und Werkstofftechnik, 37, 2006, pp. 674 – 680

[5] EN 10002-1, Metallic materials – Tensile testing - Part 1: Method of test at ambient temperature, Bruxells, 2001

[6] EN 2002-001, Aerospace series – Metallic materials – Tensile testing - Part 1: Method of test at ambient temperature, Bruxells, 2006

[7] EN 1993-1-4:2006: Eurocode 3: Design of steel structures – Part 1-4: General rules – Supplementary rules for stainless steels, Bruxells, 2006

[8] EN 1993-1-3:2006: Eurocode 3: Design of steel structures – Part 1-3: General rules – Supplementary rules for cold formed members and sheeting, Bruxells, 2006

[9] L. Gardner, D.A. Nethercot, "Numerical modelling of stainless steel in structural components – a consistent approach", Journal of structural engineering, 130, 2004, pp. 1586 – 1601

[10] A. Gehring, K. Kathage, H. Saal, SEMC 2007, 3rd International Conference on Structural Engineering, Mechanics and Computation, Cape Town, South Africa, 2007, p. 377

FABRICATION OF AISI 316LN HALF-SHELLS FOR THE SUPERCONDUCTING DIPOLES OF THE LARGE HADRON COLLIDER

F. Bertinelli[1], J. Pollmann[2], I. Rommerskirchen[2], G. Trachez[1], E. Wildner[1]

[1]CERN, European Organization for Nuclear Research, Switzerland,
[2]H. BUTTING GmbH & Co. KG, Germany

Abstract

The Large Hadron Collider (LHC) is the world's largest particle physics accelerator being built at CERN, the European Organization for Nuclear Research in Geneva, Switzerland.
The half-shells are an important structural component of the LHC dipole magnets: they present stringent quality requirements on material properties and geometry. In order to meet these requirements for the large series production, BUTTING set up a dedicated forming and machining line.
The paper describes the experience of the production process at BUTTING, specific difficulties encountered and finally a statistical correlation study between half-shell and magnet geometry.

Introduction

The LHC is a proton-proton collider housed in a 27 km circumference tunnel [1]. It is designed to provide collisions for experiments at unprecedented luminosity (10^{34} $cm^{-2}s^{-1}$) and centre-of-mass energy (14 TeV) for the study of rare particle physics events. After ten years of R&D and industrialisation and eight years of construction, the LHC is today near starting up [2], eagerly awaited by an international scientific community of over 5 000 physicists.
The main LHC components are 1 232 superconducting bending dipole magnets operating at high field (8.3 T) and therefore requiring cooling in superfluid helium at 1.9K. Each dipole consists of a cold mass, which contains the NbTi conductor carrying 13 kA, installed in a cryostat. The cold mass has diameter Ø570 mm, length 15 m and mass 30 tonnes. It is bent in the horizontal plane with a nominal radius 2 804 m to follow closely the trajectory of the particles: this corresponds to a sagitta - i.e. deviation from straight - of 9.14 mm at its centre. The outer cold mass enclosure consists of a shrinking cylinder and two end-cover extremities.
The shrinking cylinder is a structural component with several functions: containment for the superfluid helium, leak-tightness, pressure vessel at 26 bar, strength to contain the large electro-magnetic forces induced in magnet operation, stiffness to minimise internal movements. It is made from two half-shells welded together longitudinally.

The half-shells

The half-shells, or simply shells, are made from nitrogen enriched austenitic stainless steel, grade AISI 316LN. This grade shows high mechanical strength and ductility at low temperatures [3].
The shells are cylindrical half-tubes bevelled lengthways on their main edges for their welding: they have length 15 450 mm, 275 mm inner radius, thickness 10 mm, mass 1 100 kg.
The two shells are bent in opposite directions in order to achieve, after welding, the specified horizontal curvature of the cold mass, see Figure 1a. A shell pair, therefore, nominally consists

of a convex “Lower” and a concave “Upper” half-shell, with nominally 10 mm curvatures in opposite directions.
The assembly of the two shells is done in a welding press positioning the desired curvature in the vertical plane, see Figure 1b. The welding press curvature imposed by the shell supports is typically set to a sagitta of 12 – 14 mm. After welding, the combined effect of press force and controlled welding shrinkage produces a required azimuthal pre-stress of 160 MPa in the shrinking cylinder which ensures the stiffness of the cold mass, and specifically of the superconducting coil. The longitudinal welding uses a special Surface Tension Transfer (STT) technique combined with the traditional pulsed MIG welding. This mechanised process relies on a moving laser camera to reconstruct the joint geometry in order to adapt welding parameters. Consequently stringent quality and geometry requirements are placed on the manufacture of the shells, their geometry and the quality of the bevelled joint.

Figure 1. (a) schematic of half-shell curvature (not to scale), (b) a welding press at a Cold Mass Assembler

In 1999 CERN launched the procurement of components for the LHC. The purchasing strategy involved three European suppliers for the cold masses, called Cold Mass Assemblers (CMAs), Firms 1, 2 and 3. CERN decided to place separate supply contracts directly for the superconducting cable and all major components. In this context CERN negotiated a contract for the supply of all the half-shells [4] jointly with BUTTING (DE) and Icarus (BE).

The Half-Shell Production at BUTTING

The raw material

An important prerequisite for the economic production of the half-shells was the definition of optimal plate dimensions and tolerances. Based on the required final geometry and additional material to account for the machining of the bevels, the dimensions of the starting plates were specified to length 16 150 mm and width 884 mm. The plate thickness was specified more tightly to a tolerance of maximum 0.5 mm within the same plate in order to favour stability of production.
The order for the supply of the plates was placed by BUTTING with Creusot-Loire (FR), today part of ArcelorMittal. The 316LN steel was melted in an Electric Furnace (EF), processed through Vacuum Oxygen Decarburizing (VOD) and ingot cast. In view of the stringent technical specification requiring a fully austenitic microstructure with no traces of delta-ferrite, ingot casting, allowing solidification in the austenitic range with limited associated risk of hot cracking, was preferred to continuous casting. The ingots were hot rolled to a larger dimension width 1 800 mm mother plate and heat treated to the solution annealed state. Each mother plate was then shear cut longitudinally to supply two plates.

The forming process

After initial experience on an existing tube forming line, BUTTING development engineers decided to design and set up a dedicated continuous forming and machining line for the shell production. The line required to be flexible and adjustable to produce both Lower and Upper shells. It needed to use standard components, reusable after the shell production project was finished. The resulting line was over 100 m long and was housed in a dedicated assembly hall, see Figure 2a.

Production starts with the mechanical, manual measurement and recording of the dimensions of each plate, in particular the two important characteristics of plate width and wall thickness. The geometric results of the forming process were found to be extremely sensitive to the initial plate thickness: hence plates were grouped according to their wall thickness and used differently in the forming process.

The flat plates are loaded onto the forming line and joined by TIG welding to form a continuous strip. To obtain a reliable evidence of the raw material quality, ultrasonic testing is performed according to standard PrEN 10160, quality class E_4 near the edges and S_3 elsewhere.

The flat strip then feeds into a sequence of forming rollers, rotating with their axis horizontally or vertically, that progressively deforms it into a half-cylinder. This then enters a milling station where it is rigidly guided and supported for the machining of the bevel joint geometry. The two opposite chamfers are milled simultaneously, the process following the longitudinal movement of the strip. The surface quality of the produced chamfers is critical for the welding at the CMAs.

The machined half-cylinder then enters another sequence of calibration rollers and a measurement station where a laser continuously monitors the inner radius.

Finally end stiffeners are tack welded to avoid opening of the shell ends and each individual shell is cut off with a band saw. Whenever necessary the shell edges are deburred manually and the chamfer lightly polished.

BUTTING also set up custom-made stations to allow the manual calibration of the formed shells, specifically to correct for twist, curvature, straightness and radius.

Finally the shells are chemically etched to be supplied in a clean state, ready for assembly in the CMAs.

Figure 2. (a) The shells production hall at BUTTING, forming line on the left, (b) dedicated storage area

Dimensional measurements and quality control

Measurement of the shell geometry required particulare care to avoid own-weight deformation effects. Dedicated benches with special supports were set up to measure the straightness of the edges and the two curvature types. A 3-D laser measuring tracking system from Leica was used together with mechanised target movements to automate the measurement process, see Figure 3a. Dimensions measured and documented were: curvature (concave or convex), straightness and parallelism of the milled longitudinal edges, and inner radius. Measurements of

shell thickness, the inner developed length and shell length were made manually. The data was stored and recorded by BUTTING directly in the CERN quality control repository for the LHC project.

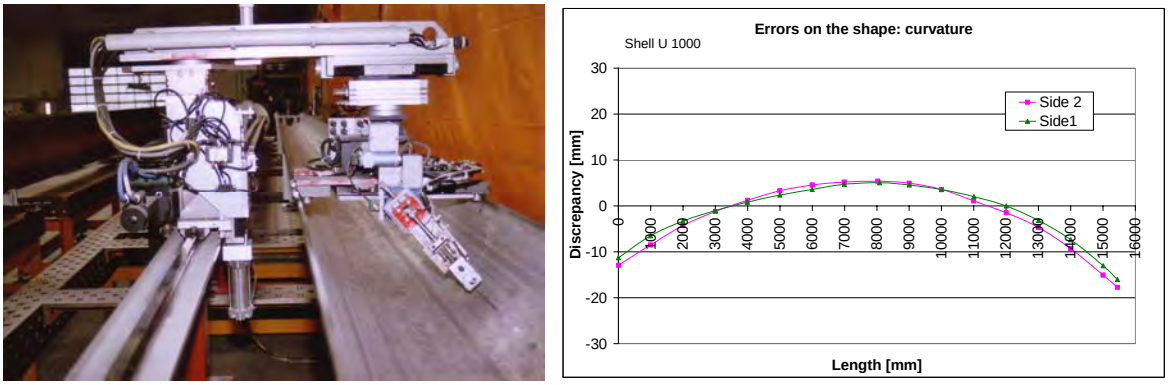

Figure 3. (a) Leica measuring sytem; (b) typical curvature results for a shell (U1000, curvature -19 mm)

Pairing of half-shells

The original pairing specified an Upper shell curvature -12.5 mm and a Lower shell curvature 12.5 mm. Since this geometry could not be achieved systematically from the forming line alone, see for example Figure 3b, BUTTING made extensive use of manual calibration. While technically effective this proved to be excessively labour-intensive and time-consuming. Moreover the CMAs reported welding difficulties associated to local misalignments between the two welding edges. It was understood that manual calibration was indeed correcting the global curvature of the shell geometry, but at the expense of introducing local discontinuities.
CERN and BUTTING had several technical discussions to review and adjust the initial specification, introducing a new concept of pairing "no-calibration" shells, see Figure 4a: this recognised that a smooth shell geometry was preferable for welding, and that curvatures of the Upper and Lower shells could compensate each other. The shell supports in the welding press could account for this new geometry, but not for the local discontinuities.
In this way shells produced from the forming line could be used directly, see Figure 4b, ultimately with benefits for both end use and for the economics of shell production.

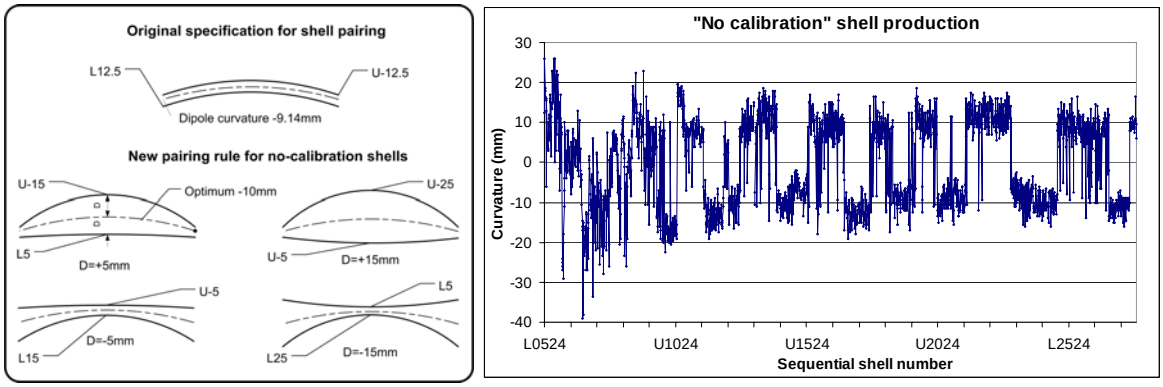

Figure 4. (a) New pairing rule for no-calibration shells with examples, (b) Curvature results showing production campaigns for Upper shells (-ve) and Lower shells (+ve) and the improvement of process control with time

Logistics

Each delivery to the CMAs consisted of 4 shell pairs, transported by truck. In full production 2-3 trucks of shells were delivered each week from BUTTING. Due to the continuous production of Lower and Upper shells and the need to pair them, stock levels rose up to 600 shells, see

Figure 2b: accordingly BUTTING dedicated a separate storage area to the finished products. Adequate packing suitable for storage and transport required particular attention. The final shell pairs were delivered in December 2006.

Statistical studies of shell and cold mass geometry

Shell production

A specific production difficulty was to control the parameters of the forming line in order to achieve the correct shell curvature. After an initial learning period, BUTTING was successful to establish settings that could produce the desired Upper or Lower shells repetitively.
Occasionally, however, a few "outlier" shells presenting a completely different curvature were produced, see Figure 6.

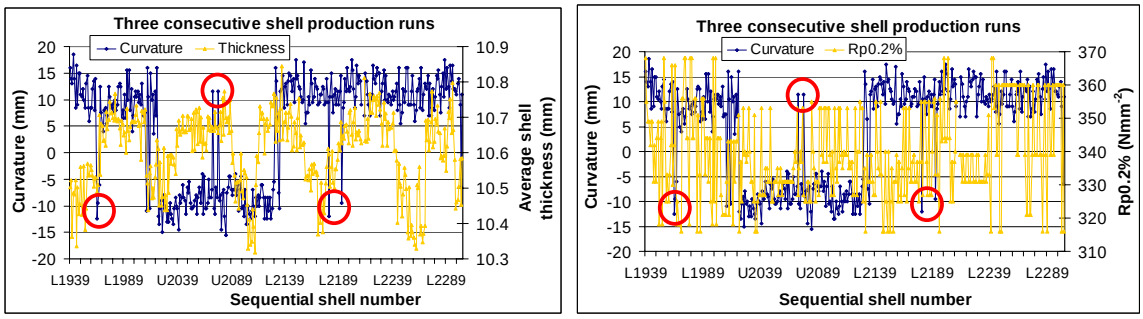

Figure 6. Presence of shell "outliers" in production:
no correlated effect from (a) shell thickness and (b) material properties

With all settings constant, this occasional behaviour most probably originates from the plate characteristics. A statistical analysis of shell thickness and plate material properties did not show any evidence towards these two characteristics being the source of the problem. The unusual behaviour is probably associated to a more technological plate property, possibly flatness or residual stresses.

Shell pairing and effect on cold mass geometry

The quality of pairing of no-calibration shells is characterised by two parameters: the curvature of the shell pair (specified $-10^{\pm 0.5}$ mm) and the deviation of shell pairs from nominal D (mm), see Figure 4a. Further criteria include the shell straightness in order to minimise difficulties of CMAs during welding due to poor edge alignment.
Naturally the quality of pairing improved as the control of production of no-calibration shells improved, see Figure 7a.
Shell pairs were not delivered equally to the three CMAs: Firm 1 was supplied most of the high value +ve and -ve D shell pairs, while Firm 3 who had the most aggressive production schedule almost exclusively low D pairs, see Figure 7b.

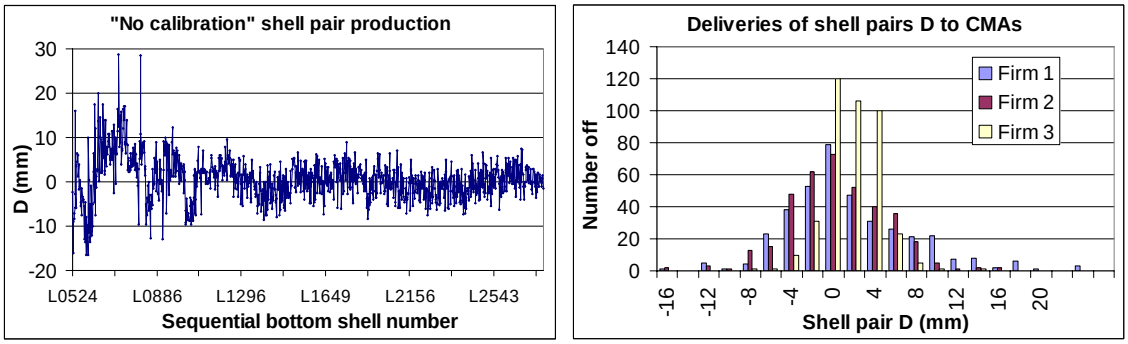

Figure 7. (a) "D" characteristic of shell pairs, (b) "D" shell pairs as supplied to the three CMAs

The geometry of the assembled cold masses is also measured - with similar 3D Leica technology as used for the shells - specifically after the longitudinal welding (ITP15), after the endcover welding (ITP20) and after transport to CERN and cold testing (WP08): results are expressed in terms of "delta sagitta", i.e. deviation from the nominal cold mass sagitta 9.14 mm. Two characteristics are particularly important: cold mass curvature and cold mass geometry stability. Several factors affect these characteristics: the welding press curvature settings, stiffness of assembly of the components inside the cold mass, correction of cold mass support positions at CERN and possibly shell pair geometry.
When considering average values over all production, the shell pairs and the corresponding cold masses show similar trends (but clearly this does not necessarily imply a cause-effect relationship): shell pairing D with cold mass stability, see Figure 8b, and shell pair curvature with cold mass curvature, see Figure 8d. For example, cold masses from Firm 1 show the relatively "worst" geometry stability (with a small increase in curvature after transport and cold testing) and the highest value of shell pairing D. Cold masses from Firm 3 show the "largest" curvature and the largest curvature of shell pairs.

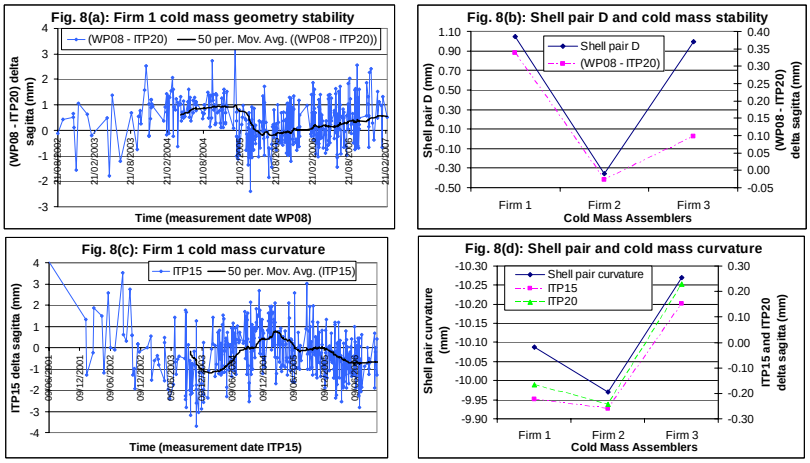

Figure 8. (a, b) cold mass geometry stability and (c, d) cold mass curvature

However no one-to-one correlation can be found between individual shell pairs and their corresponding cold mass geometry, most likely since several contributing factors exist. In particular there is no visible effect of large +ve and –ve D shell pairs. Therefore there is only weak evidence for a contribution of the geometry of the supplied shells to the final geometry of the cold masses.

Conclusions

BUTTING was successful in supplying shells to the requirements of CERN and the Cold Mass Assemblers, while satisfying the economics of series production. The close collaboration between CERN and BUTTING engineers allowed to adapt the initial stringent specification while focussing on the few essential criteria. The geometry of the shells as produced and paired was shown to be acceptable to ensure the precision of the final geometry of the cold masses.

References

[1] LHC Design report, Vol. 1 “The LHC Main Ring”, CERN-2004-003, June 2004.
[2] L. Evans, “LHC Status”, APAC 07, Indore, India, February 2007.
[3] K. Couturier, S. Sgobba, Proceedings of the "Materials Week" European Conference, Munich, Germany, September 25-28, 2000.
[4] F. Savary, “Technical Specification for the supply of austenitic stainless steel shells for the cold masses of the LHC superconducting dipole magnets”, CERN, EDMS 103374, June 1999.

DEVELOPMENT OF HIGH STRENGTH NON-MAGNETIC DRILL COLLAR DNM140

K. Ishikawa, T. Shimizu

Daido Steel CO., LTD., Japan

Abstract

In recent years, there has been a growing demand for oil due to the increase of energy use worldwide. Thereby the rise of the oil price has been induced, and it has triggered a new boom in the petroleum industry. This boom is facilitating the exploration of new oilfields and the application of more advanced technology for petroleum drilling and production. However, the drilling environment is severe, so that drill collars need to be stronger, tougher and more corrosion resistant. To satisfy these new requirements, a new austenitic stainless steel with high strength, toughness and excellent corrosion resistance has been developed by optimizing the chemical composition of Cr-Mn austenitic stainless steels and by warm working.

Introduction

The rise of oil prices over the past several years has inspired new activities in oil exploration operations. Especially the method of directional drilling combined with measurement while drilling (MWD) has permitted exploration of reservoirs to which access was unthinkable in the past, and resulting in a lot of new oil fields in the world [1].

In order to lead to new reservoirs, both MWD and the logging while drilling (LWD) measure the magnetic field of earth for navigation and the identification of geological formations. These systems send the data to the base on the surface. Therefore the drill collars need to be non-magnetic, have high corrosion resistance for the aggressive environment in the oil well, and high strength to withstand the extreme force in the downhole. Only nitrogen alloyed austenitic stainless steels and nickel-based alloys satisfy these requirements for this application [2].

Manufacture of non-magnetic drill collars

The production of non-magnetic drill collars is carried out consecutively in Daido Steel. Figure 1 gives an overview of the stages of fabrication. The melting is done in a 20t electric arc furnace. Then, ingots are cast. These processes are continued under atmospheric pressure. The ingots are hot forged by a forging press. These drill collar pre-materials are warm-worked after solution

treatment, and then machined and inspected. Finally final machining is carried out final machining by customers.

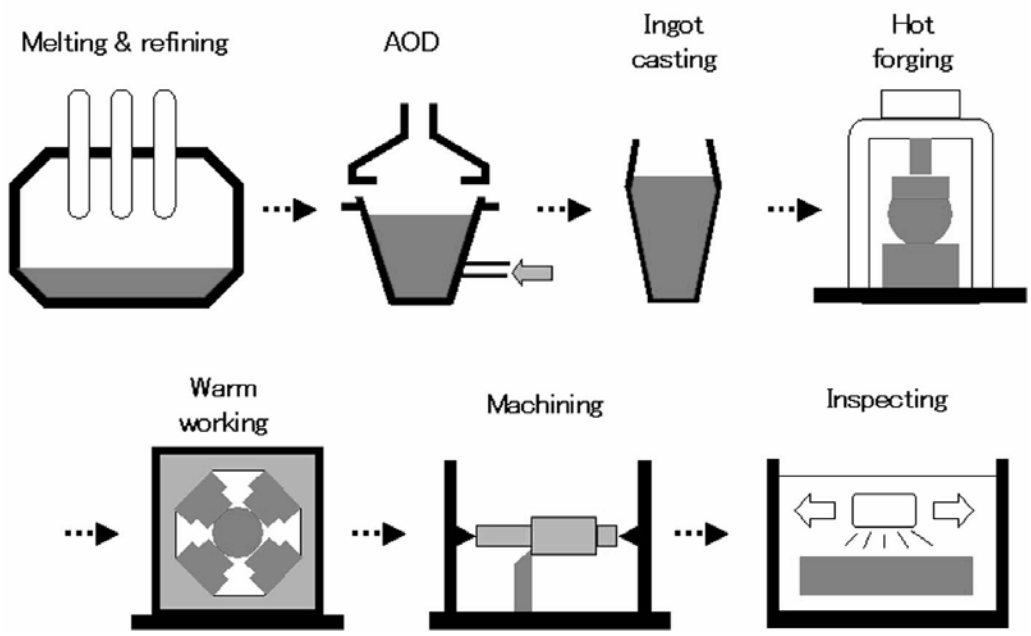

Figure1. Manufacture process at DAIDO STEEL

Development of DNM140

In order to fulfill new requirements for drill collars, we have developed a new non-magnetic austenitic stainless steel DNM140 possessing high strength and high corrosion resistance. The chemical composition of the steel is shown in Table 1. High strength is given to this steel by solid solution strengthening of interstitial nitrogen and by the warm working [3]. The high corrosion resistance is obtained by the use of chromium, molybdenum and nitrogen [4]. In this text, we introduce the characteristics of DNM140 as follows.

Table 1. Chemical composition of DNM140 (typical values).

C	Si	Mn	P	S	Cu	Ni	Cr	Mo	N
0.03	0.29	15.7	0.022	0.001	0.36	3.2	18.6	0.83	0.48

(mass%)

Characteristics of DNM140

The samples for the investigations of corrosion resistance and mechanical properties have been taken from bars, which were warm worked after the solution treatment. The fundamental magnetic properties were taken from cold worked bars.

Magnetic properties

The steel for drill collars have to be strictly non-magnetic, because they manage very sensitive electronic devices. Its permitted maximum value is μ=1.005 in 200 Oe.
Table 2 shows the relative magnetic permeability in 200 Oe of DNM140, which is measured with the sample extracted 1 inch below the surface. Both sizes have very low value. Figure 2 shows the magnetic permeability to each cold reduction. It is seen that even at the 80 percent cold reduction, the magnetic permeability remains less than 1.005.

Table 2. Magnetic properties

	6-3/4"	8"
Relative Magnetic Permeability (200 Oe)	1.002	1.003

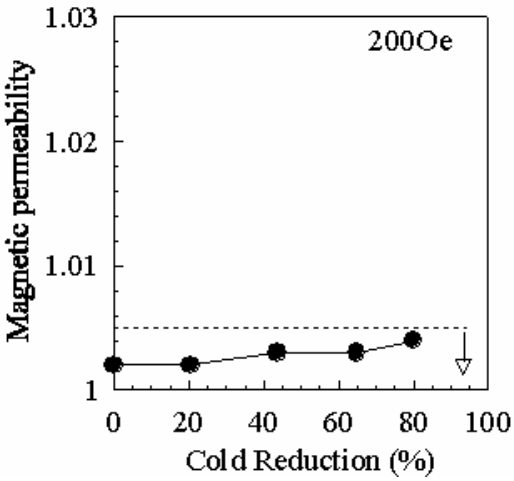

Figure 2. Effect of cold reduction on magnetic permeability

Corrosion properties

The microstructure of DNM140 is fully austenitic, and it possesses good resistance to both inter-granular corrosion and SCC.

Oxalic acid etch test for classification of etch structure (ASTM A262 Practice A)

The microstructure of DNM140 is fully austenitic, so neither ferrite nor strain-induced martensite can be found. In order to reach good corrosion resistance and ductility properties, it is also important to avoid the precipitation of chromium nitrides and carbides. As shown in Figure 3, this structure is suitable for non-magnetic drill collars.

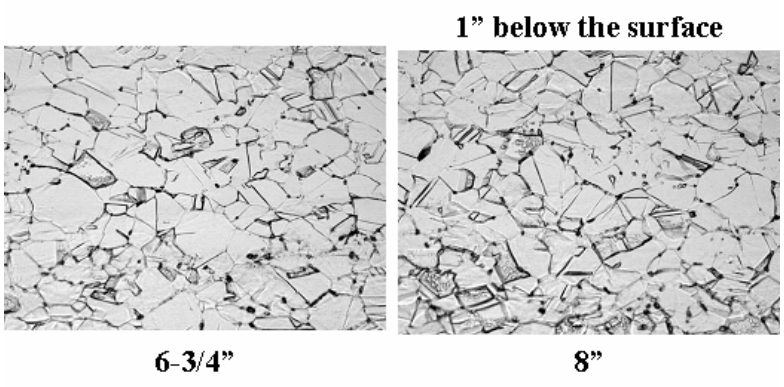

Figure 3. Results of the oxalic acid etch test

Copper-copper sulfate-16% sulfuric acid test (ASTM A262 Practice E)

In order to characterize the susceptibility to intergranular attack, a copper-copper sulfate -16% sulfuric acid test was carried out. This test detects susceptibility to inter-granular attack associated with the precipitation of chromium-rich carbides. The test coupons have no cracks even after 180°bending (Figure 4).

	* Inside the bore	
	6-3/4"	8"
Corrosion Cracking Resistance ASTM A262 Practice E	No cracks (180˚ bend)	No cracks (180˚ bend)

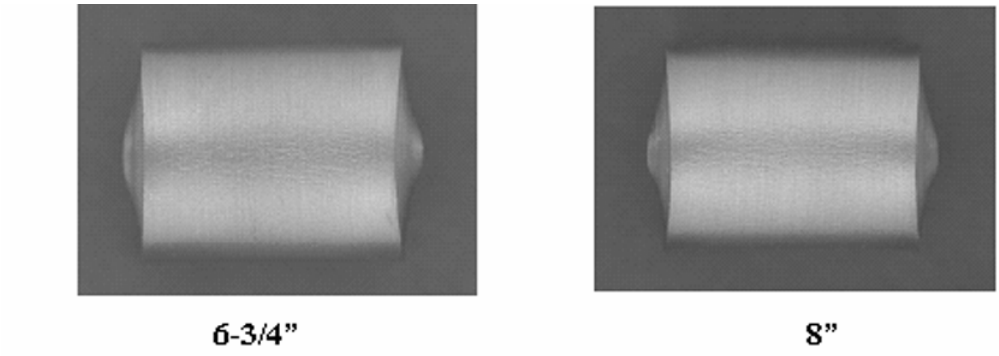

Figure 4. Results of copper-copper sulfate-16% sulfuric acid test

SCC Resistance (ASTM G36)

In order to characterize the resistance against stress corrosion cracking a constant load test in boiling 45 wt% $MgCl_2$ at 155°C was carried out. The results of stress corrosion resistance are shown in Figure 5. The rupture life of DNM140 is more than 300 hours without cracking at the applied stress of 400 MPa.

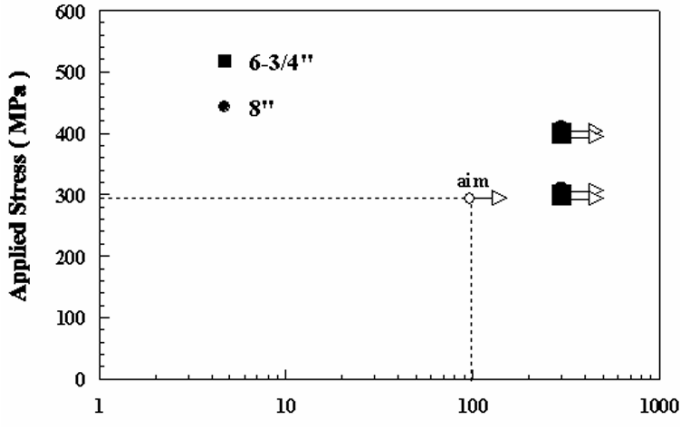

Figure 5. Results of stress corrosion tests in 45 % $MgCl_2$ at 155℃

Measurement of pitting potential

In order to evaluate the resistance against chloride-induced pitting corrosion, anodic polarization curves have been recorded. The tests were carried out at a temperature of 30°C in 3.5 % sodium chloride solution. Figure 6 shows pitting corrosion potential against the saturated calomel electrode at a current density of 10^{-4} A/cm^2. A pitting corrosion potential of DNM140 for a 3.5% sodium chloride solution can be achieved with 400 mV. This potential is higher than for Type 304 and Type 316. Hence, DNM140 has good resistance against chloride-induced pitting corrosion.

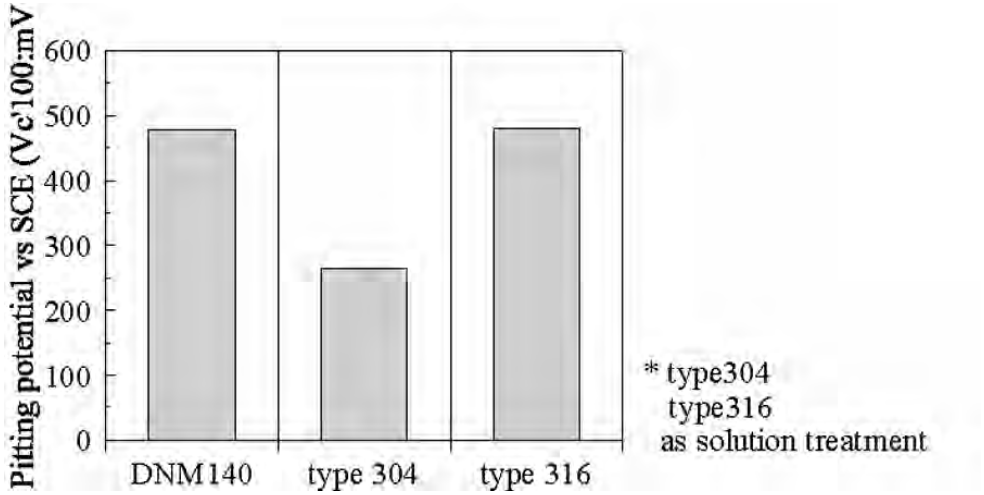

Figure 6. Results of pitting potential tests

Mechanical properties

The specimens for tensile tests and Charpy impact tests were taken from the warm worked bars at 1 inch below the surface. The values of the results are shown in Table 3, the 0.2% yield strength of DNM140 is more than 140 ksi (965 MPa), and the ultimate tensile strength is more

than 150 ksi (1034 MPa). Further, the Charpy impact value for V-notch specimens is more than 100 ft-lbs (136 J).

Table 3. Mechanical properties

	6-3/4"	8"
0.2% Yield Strength ksi	142	152
Ultimate Tensile Strength ksi	158	164
Elongation %	30	27
Charpy Impact Value ft-lbs	135	120

Summary

DNM140 is a non-magnetic steel having 0.2% proof stress more than 140 ksi (965 MPa) and high corrosion resistance. They certify that DNM140 fulfills the requirements to use the steel in the drilling technology application of the petroleum industry.

References

[1] J.N. Cordea, HV. Sheth, J.C. Jasper: Materials Performance, 1987, p. 50

[2] A. Ikeda, T. Kudo, Y. Okada, S. Mukai and F. Terasaki: Corrosion/84, Paper No. 206, 1984 (NACE)

[3] H.H. Ulig, Trans. Am. Soc. Met, Vol. 30, 1942, p. 947

[4] J.E. Truman: Proc. UK Corrosion'87, 1987, p. 111.